ETH
Eidgenössische Technische Hochschule Zürich
Swiss Federal Institute of Technology Zurich

Quantum Device Lab

Semester Thesis

Characterizing the thermalization and attenuation of microwave waveguides at cryogenic temperatures

Nicholas Meinhardt

March 28, 2018

Supervisor
Philipp Kurpiers

Professor
Prof. Dr. Andreas Wallraff

Abstract

Transmitting photons with low loss between distant qubits is essential for most implementations of quantum processing. We characterize the frequency and input power dependent loss of a commercially available rectangular microwave-frequency waveguide that has been shown to be well suited for our purposes in previous studies. Using a resonant-cavity technique, we obtain attenuation constants down $0.6\,\mathrm{dB\,km^{-1}}$ (a transmission of 99.986 % of the signal over 1 m) for an uncoated aluminium 6061 waveguide WR90 with a length of 3650 mm at temperatures between 80 mK and 130 mK. To achieve low loss and low thermal excitation of modes at the used frequency 8.35 GHz the waveguide needs to be well thermalized. We discuss thermal clamps as a way to establish a good thermal contact between the waveguide and base temperature shield. We optimize the length of the braids with respect to thermal expansion of several components of the system and tune the thermal contact between waveguide and braids by changing the thickness of steel plates. Despite these efforts we still measure a temperature difference to the shield of 80 mK due to the small thermal conductivity of Al in the superconducting phase.

Contents

1 Introduction **4**

2 Analysis of thermal expansion of waveguide-related components **4**
2.1 Thermal clamps 4
2.2 Waveguide and shield 6
2.3 Setup for measuring thermalization 9
2.4 Thermalization measurement 9

3 Experimental setup for measuring the attenuation constant **12**

4 Results **13**
4.1 Measurements at RT 13
4.2 Measurements at cryogenic temperatures 13

5 Conclusions **16**

Appendix A Linear thermal expansion parameters **17**

Appendix B Displacements at several positions **17**

Appendix C Mode numbers of resonance frequencies at RT and BT **18**

Appendix D Analysis of the rectangular waveguide **18**

Appendix E Background and noise level **19**

Appendix F Measured external Quality factor **20**

Appendix G Influence of optical Kerr effect on waveguide modes **21**

References **23**

1 Introduction

For quantum information processing it is necessary to entangle distant qubits and create a quantum channel for the communication between them with a low attenuation [1]. Experiments using circuit quantum electrodynamics have shown that single microwave photons can be used for a coherent interaction with qubits [2–4]. Most protocols require the ability of transmitting a microwave photon with low loss to increase the fidelity or the rate of entanglement generation [1]. Thus it is essential for distributed quantum computing to study the loss of quantum channels and to minimize it. In previous studies, the attenuation constants of different types of microwave-frequency coaxial cables and rectangular waveguides were estimated down to $0.005\,\mathrm{dB\,m^{-1}}$ and temperatures of tens of millikelvin using drive powers down to single photon level [5]. To extract the frequency dependent loss within frequency ranges of 3.5 - 12.8 GHz the resonant cavity technique was used. The rectangular waveguide of type WR90 by Electronic Industries Alliance (EIA) standard out of uncoated aluminium 6061 was measured to be a well suited device to reduce the loss in a frequency range around 8.3 GHz. The waveguide manufactured by Penn Engineering Components, Inc. [6] has inner dimensions of 22.86 mm and 10.16 mm and a recommended frequency band of 8.2 to 12.4 GHz.

In experiment presented here we chose WR90 of lengths 1150 mm and 2500 mm. At room temperature (RT) we performed measurements of the attenuation constants of each part. Furthermore, we performed the same measurements at cryogenic temperatures of tens of millikelvin with the both parts screwed together, which is the first time that we analysed the whole setup of length 3650 mm.

In the first part of this thesis we discuss the way we thermalize the waveguide to nominally a few tens of millikelvin and how we can optimize the lengths of the braids that are used for thermalization. For that purpose we investigate the influence of thermal expansion on several parts of the system. In the second part we study the frequency and input power dependent loss of the waveguide at RT and cryogenic temperatures using the resonant cavity technique.

2 Analysis of thermal expansion of waveguide-related components

In order to initialize the quantum systems close to their thermal ground state, they are placed in a cryogen-free dilution defigerator system, which achieves temperatures of around 10 mK at the base temperature (BT) stage. We thermally anchor the waveguide at several positions to the BT shield using copper braids (CU-OF) and clamps. The waveguide is supported by holders which are fixed to the BT shield.
For optimizing the lengths of the thermalization braids and the thermal connectivity between braids and waveguide we discuss the effects of thermal expansion on several waveguide-related components in this section.

2.1 Thermal clamps

A first requirement is to increase the thermal conductivity between waveguide and braids to obtain a good thermal connection between BT shield and waveguide. Therefore, it is essential to mount the braids and the waveguide with a high pressure to reduce the contact resistance [7]. This is performed using thermal clamps that are schematically shown in Fig. 1. The clamps consist of two plates and screws that enclose the waveguide and the braids. Since the thermal expansion of aluminium is larger than of brass, the contact pressure decreases during the cooldown process. Using plates out of stainless steel we can

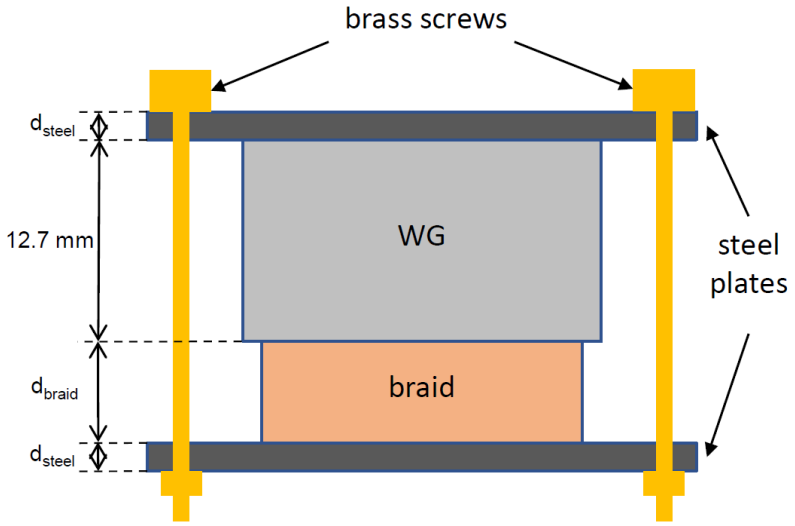

Figure 1: Scheme of the clamp to thermalize the waveguide. The waveguide and the copper part are placed between two steel plates, their thicknesses are displayed as d_{steel}, d_{braid} and d_{WG} which is fixed. Screws out of brass press the plates together.

account for that and increase the contact pressure at cryogenic temperatures, because steel contracts less than aluminium and brass. We calculate the minimum thickness d_{steel} of the plates to compensate for the effect described above. Moreover, we ensure that the screws do not break due to thermal stress exceeding the limit for reversible deformation resulting in an upper limit for d_{steel}.
For the upper limit we consider the stress on the screws at a given temperature, which is induced by the different actual lengths of brass and the combination of waveguide, braids and both plates. Knowing the Young's Modulus $E_{\text{brass}} \approx 100$ GPa of brass and assuming that it is temperature independent, we can directly relate the strain $\varepsilon = \frac{\Delta l}{l}$ to the stress σ as

$$\sigma(T) = E_{\text{brass}}\varepsilon(T) + \sigma_{\text{pre}} = E_{\text{brass}}\frac{\Delta l(T)}{l(T)} + \sigma_{\text{pre}}, \tag{1}$$

where $l = 12.7\,\text{mm} + 2 \cdot d_{\text{steel}} + d_{\text{braid}}$ is the thickness of waveguide, braid and steel and Δl is the difference between l and the brass screw length l_{brass}

$$\Delta l = l - l_{\text{brass}} = \alpha_{\text{aluminium}} \cdot 12.7\,\text{mm} + \alpha_{\text{copper}} d_{\text{braid}} + \alpha_{\text{steel}} d_{\text{steel}} - \alpha_{\text{brass}} d_{\text{brass}}. \tag{2}$$

At RT, $d_{\text{brass}} = l$ and the linear expansion coefficients α are the ratios of the length variation due to thermal expansion and the actual length of each material as discussed in section A of the appendix. If the stress exceeds the Yield's strength $\sigma_{\text{Y}} \approx 200$ MPa of brass, the screws start to deform. Thus the applied stress has to stay below σ_{Y} to be stable, defining the upper boundary. Tightening the screws during assembly results in a prestress σ_{pre} at RT. Comparing our M3×0.5 brass screws with steel screws of strength category 4.6 in a prestressing force table [8] and dividing by the cross section of the plates yields a prestess of approximately 5.6 MPa.
Fig. 2 shows the stress as a function of temperature T. The Yield strength σ_{Y} is indicated as red dashed line that should not be crossed and we neglect a possible temperature dependence. Considering large d_{steel} we neglect the other materials and approximate the system as only consisting of one block of steel and the screws. This limes is represented by the green and purple dashed curves, for σ_{pre} of 5.6 MPa and 115 MPa, respectively. In the limit of a vanishingly small d_{steel}, which corresponds to the initially mentioned challenge with not plates present, we plotted $\sigma(T)$ with the yellow curve. We assume $d_{\text{braid}} = 1$ mm

for the thickness of the braids. Moreover, the stress for $d_{\text{steel}} = 2\,\text{mm}$ and $\sigma_{\text{pre}} = 5.6$ MPa is plotted in blue.
To stay in the reversible regime even for large d_{steel} the prestress must not exceed 115 MPa. For $\sigma_{\text{pre}} < 115$ MPa the thickness of the plates does not effect the stability, because Δl also scales with l, resulting in the first term in Eq. 1 being a constant which is small compared to σ_{Y}. As the expected prestress we obtain due to assembly is below the limit, we are able to choose arbitrarily large d_{steel}.
The minimum thickness requires an increase of σ when being cooled down to BT, so that $\sigma(T) > 0$ or $\Delta l(T) > 0$ if we neglect the prestress in Eq. (1), respectively. According to equations 1 and 2 the minimum value for d_{steel} depends on d_{braid}. Assuming $d_{\text{braid}} = 1$ mm we derive the condition $d_{\text{steel}} > 1.94\,\text{mm}$ and therefore use 2 mm in the experiment.

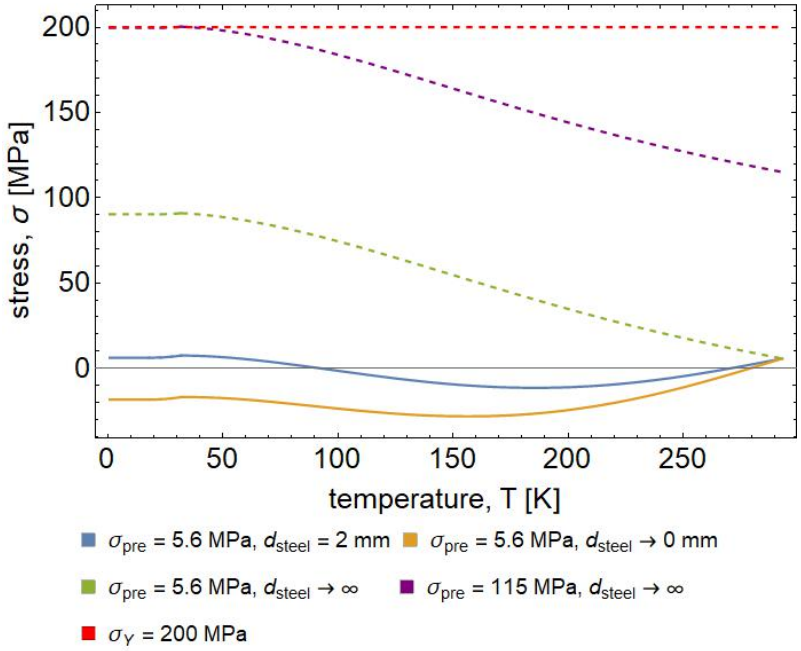

Figure 2: Stress σ versus temperature T for several prestresses σ_{pre} and thicknesses d_{steel} of the steel plates, assuming a thickness $d_{\text{braid}} = 1$ mm of the braids.

2.2 Waveguide and shield

A schematic of the waveguide thermalization for later experiments is shown in Fig. 3 both at RT and BT. The connection module (CM) of length 1.25 m connects a cryostat to the horizontal link consisting of several shield modules (SM) of length 2.5 m. As represented by the dashed black lines, each SM is assumed to contract towards its center and each CM is fixed at a cryostat. The waveguide is fixed across from the cryostat as indicated by the solid blue line, such that it contracts towards the direction away from a cryostat. It is thermally connected to the BT shield at several positions x (Fig. 4) using the thermal clamps discussed above.
Due to thermal expansion, each segment contracts towards its fixed point while cooling down the system, indicated by the red arrows in both figures. In Fig. 4, Δs is the distance along the x-axis between the connection points of braids and waveguide or BT shield, respectively. As one can see in the schematic, Δs depends on T, which must be taken into account for the braid lengths.
Fig. 5 shows Δs at BT versus position, where we assumed $\Delta s = 0$ at RT, and the length

differences Δx between RT and BT. Within each segment of the shield Δs varies linearly as indicated by the red dashed line. We extract a slope of $-0.9\,\mathrm{mm\,m^{-1}}$. The dashed vertical lines correspond to the positions of the waveguide clamps (appendix A).
Knowing Δs we can match the lengths of the braids for thermalization with the positions at the shield.

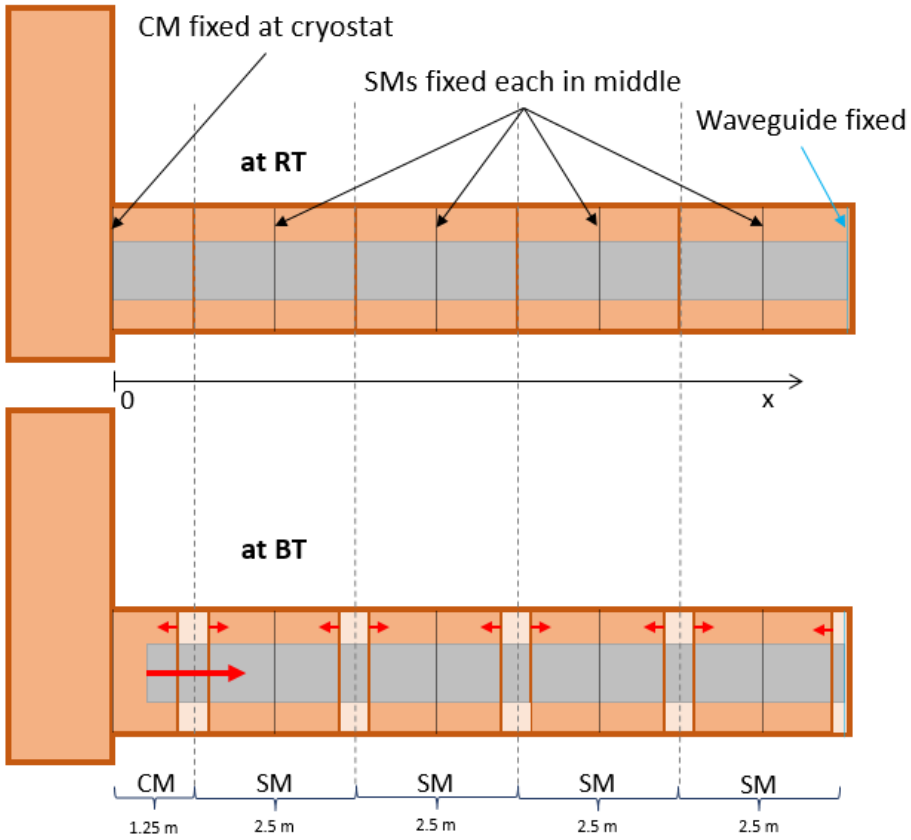

Figure 3: Schematic of the system at RT and BT. The connection module (CM) connects the cryostat and the shield modules (SM), the waveguide is enclosed by the shields. As indicated by the red arrows, the waveguide is assumed to contract away and the CM towards the cryostat, the SMs contract towards the middle.

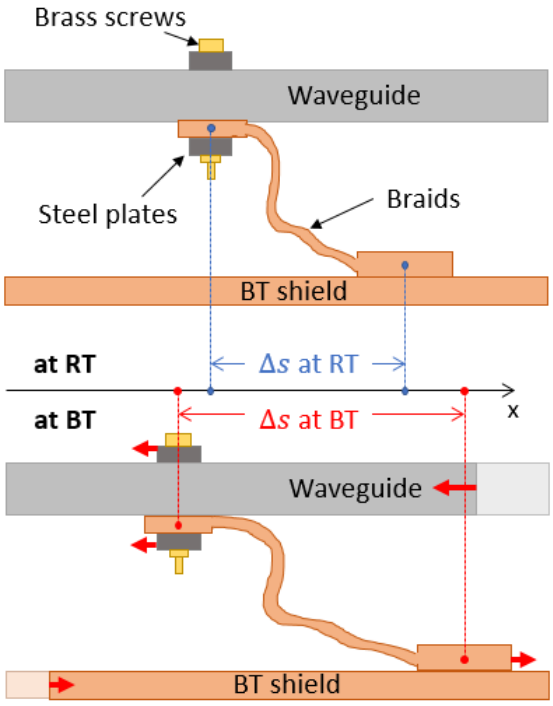

Figure 4: Schematic of the thermal connection of waveguide and BT shield by braids using thermal clamps. At RT and BT the positions of the connection points differ due to thermal expansion, Δs is the length difference along x between these points.

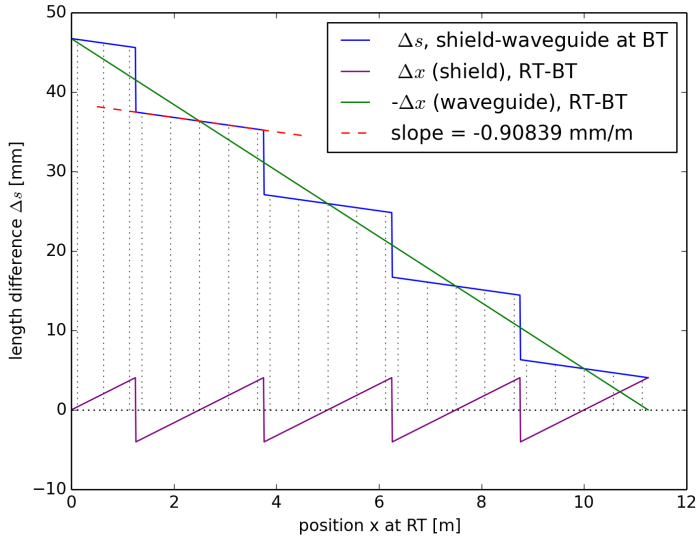

Figure 5: Plot of length differences due to thermal expansion from RT to BT. The blue line corresponds to the difference Δs between shield and waveguide at BT assuming $\Delta s = 0$ at RT, the green and violet curves display the difference Δx between RT and BT for both components.

2.3 Setup for measuring thermalization

In this section we discuss the performance of thermalization. We obtain the actual waveguide temperatures by measuring the resistance of calibrated Ruthenium oxide (RuO) sensors that are mounted at the BT plate as a reference and at the top of a 125 mm piece of the waveguide. Moreover a heater is mounted at the top, so that we can apply a certain heat load and measure the resulting temperature difference between the top of the waveguide and the BT plate. The waveguide is placed on the BT plate as one can see in Fig. 6.
For comparison, we thermally anchor the waveguide in three different ways. In Fig. 6a we screw the waveguide on the BT plate on the bottom. In Fig. 6b and c we use braids and the clamps discussed above for thermalization without tightening the screws connecting the waveguide and the BT plate. In b untreated braids are used (V1), whereas in c we adapt the part that is connected to the waveguide by pressing copper blocks around and polishing it (V2). The braids are fixed on the BT plate.

2.4 Thermalization measurement

For the described three setups we measure temperature differences in relation to the applied heat load as plotted in Fig. 7. As a reference, we plotted the dashed curve for Al1100 from literature for comparison.

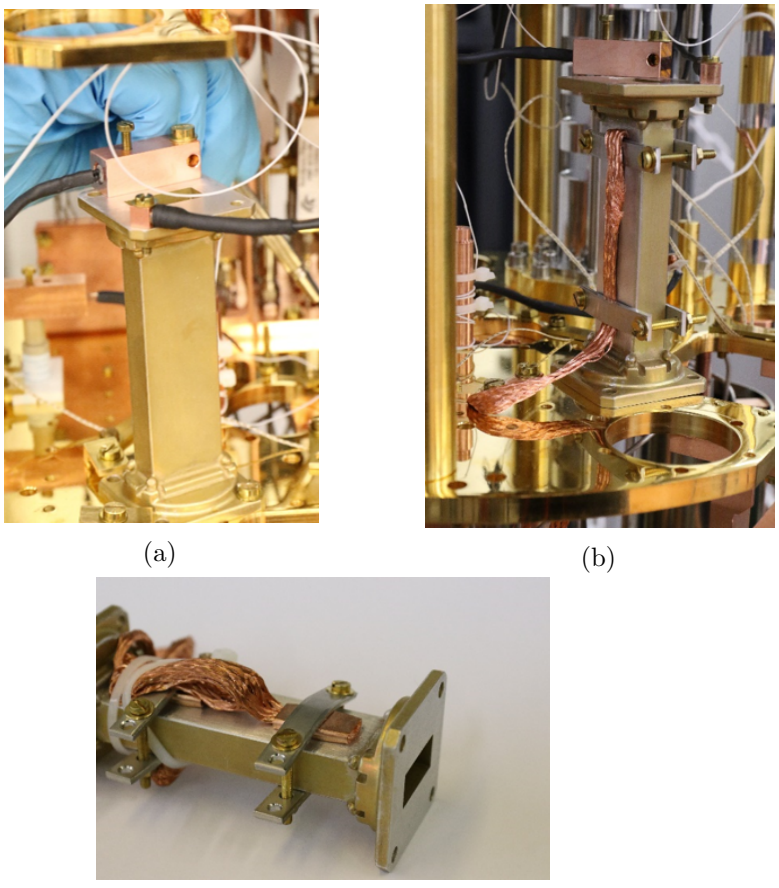

(a) (b)

(c)

Figure 6: Experimental setup to measure the thermalization of a 125 mm piece of the waveguide. In (a) a waveguide of length 125 mm is screwed on the BT plate. In (b) untreated braids and thermal clamps are used for thermalization, whereas in (c) copper blocks are pressed on the braids and the contact surface with the waveguide is polished.

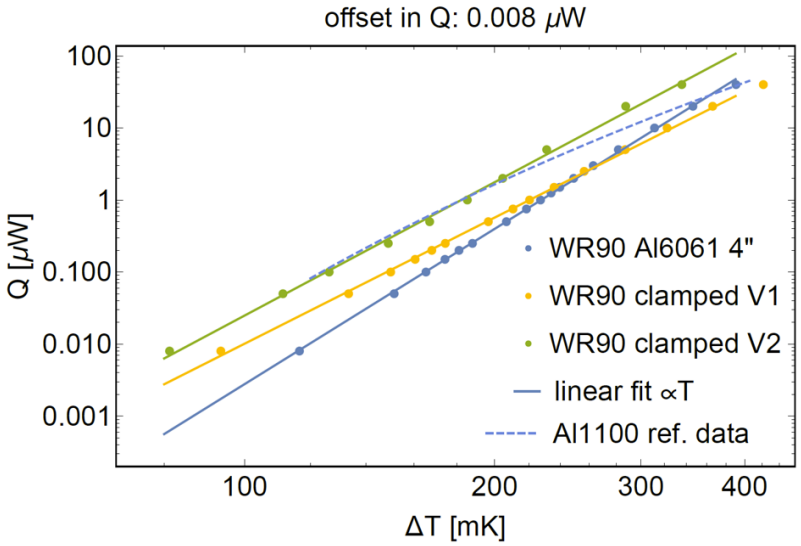

Figure 7: The measured temperature differences ΔT between the top of the waveguide and the BT plate are plotted versus the applied heat load Q for three different setups discussed in the text. Literature data for Al 1100 are plotted as reference. Fitting the data yields a power law of $\Delta T \propto Q^{-4}$ as displayed by the solid lines. The data plotted at $Q = 0.008\,\mu\mathrm{W}$ correspond to no applied heat, the Q value is chosen according to the fitting model of the unclamped waveguide represented by the blue line.

V2 has the best thermalization properties within our range of Q, implying that the thermal contact of a polished and pressed contact surface is better than one of an untreated surface. Both versions with thermal clamps have a smaller ΔT for a certain heat load below 1 µW than the version without clamps and braids.
Fitting the data for each version as displayed by the solid lines yields a power law of approximately $\Delta T \propto Q^{-4}$. Although not applying any heat, we still measure a ΔT of around 80 mK in all samples, corresponding to $Q = 0.008\,\mu\mathrm{W}$ on the fitted curve of the waveguide without braids. This Q conforms to the radiative load of the 1 K plate above the BT plate. For V1 and V2 the measurements without applied heat are also plotted at this Q. A reason for the finate ΔT is the bad thermal conductivity of aluminium in its superconducting phase at temperatures $T \ll T_\mathrm{c} = 1.2\,\mathrm{K}$.
This can be seen when solving the heat equation for the waveguide between two clamps at a distance of 500 mm and assuming a well working thermal connection to the BT plate at the clamps. The theoretical temperature in the middle of both clamps as a function of time is shown in Fig. 8. Here we assume a temperature of 20 mK at the clamps and 1 K in the middle at $t = 0$. Even after long time scales like a week and longer, the temperature in the middle significantly differs from the nominal value of the tens of millikelvin at the BT plate. Varying the distance between the clamps, we achieve nearly the same results, yielding that the distance does not effect the thermalization considerably. Thus, using only braids and clamps at discrete positions with distances of the order of 100 mm, we obtain temperatures of the waveguide of around 80 mK.
An alternative might be to cover the waveguide completely with a film of a non superconducting material with good thermal conductivity such as copper. The disadvantage of this option is the weight, since a light waveguide is a desirable for the porous posts of the shields.

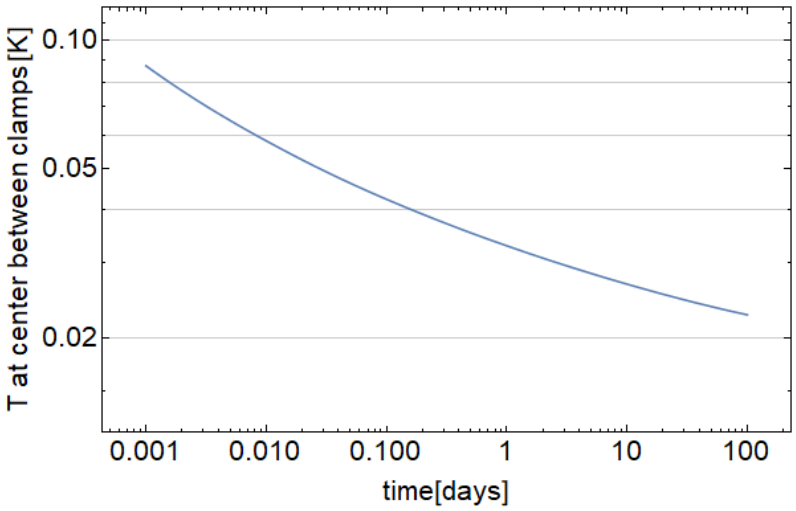

Figure 8: Solving the heat equation for an aluminium waveguide of length 500 mm in its superconducting phase yields the displayed time dependence of the temperature T in the middle of two thermal clamps. As temperature at the ends 20 K are assumed.

3 Experimental setup for measuring the attenuation constant

For measureing the attenuation constant we build a resonator from our rectangular waveguide. By installing aluminium 1100 plates of thickness 3 mm with a center hole of radius 4.1 mm between the waveguide and the input and output couplers we inductively couple the rectangular 3D cavities [9] as displayed in Fig. 9 (a). The coupling aperture is tuned such that Q_e is much larger than the internal quality factor Q_i to allow for a precise measurement of Q_i. The fitting model to extract Q is discussed in the appendix D.
At RT we use a vector network analyser (VNA) to measure the complex transmission S_{21}. To account for losses and phase offsets in the interconnecting cables we set the reference plane to the input and output coupling ports using a through-open-shot-match (TOSM) calibration. A scheme of the setup at RT is shown in Fig. 9 (b).
The setup at cryogenic temperatures is schematically shown in Fig. 9 (c). The input signal passes a chain of attenuators of 20 dB at the 4 K, cold plate (CP) and BT stage before it reaches the waveguide, the output signal passes an isolator with a frequency range of 4-12 GHz and an isolation larger than 20 dB. Then the output signal is amplified by a high-electron-mobility transistor (HEMT) amplifier with a bandwidth of 1-12 GHz, a gain of 40 dB and a noise temperature of 5 K, as specified by the manufacturer. At RT the output signal is further amplified and demodulated, the signal is digitised and the amplitude averaged using a field programmable gate array (FPGA) [10] with a custom firmware.
The waveguide is thermalized to a temperature of 80 mK to 130 mK in the way discussed in the previous section.

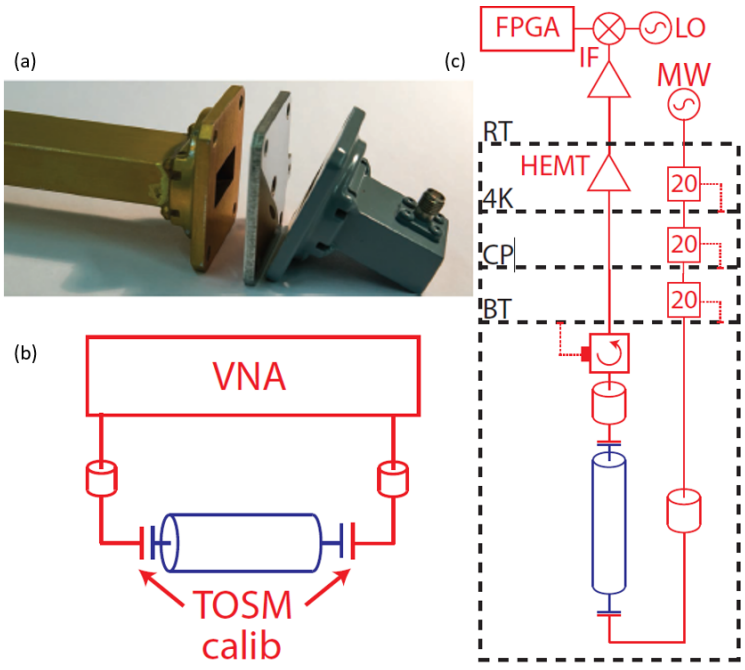

Figure 9: [5] Photograph (a) of the aperture coupled waveguide. Schematics (b) and (c) display the setups used for RT and cryogenic temperatures, respectively. At RT we use a through-open-shot-match (TOSM) calibration to account for losses and phase offsets in the interconnecting cables and a vector network analyser (VNA) to measure the complex transmission. At cryogenic temperatures a FPGA-based microwave setup is used.

4 Results

4.1 Measurements at RT

The measured transmission $S_{21}(\nu)$ for the 2500 mm waveguide is shown in Fig. 10, where we measured the spectrum between 6 GHz and 16 GHz. The peaks correspond to the modes we discuss in our analysis in section D of the appendix. The first modes of the 1150 mm and 2500 mm waveguides start accordingly to theory at a frequency of around 6.5 GHz.
A plot of the extracted resonance frequencies of the 1150 mm and 2500 mm waveguides versus their mode numbers can be found in the appendix E. The extracted quality factors Q from the fits and the calculated attenuation constants α are plotted in Fig. 11 for both lengths of the waveguide. We extract quality factors of around 6000 and attenuation constants of around $0.07\,\mathrm{dB\,m^{-1}}$ for the 1150 mm waveguide and $0.17\,\mathrm{dB\,m^{-1}}$ for the 2500 mm one. We assume that the fluctuations in Q and α for the longer waveguide are caused by an imperfect calibration and standing waves in the input and output couplers.

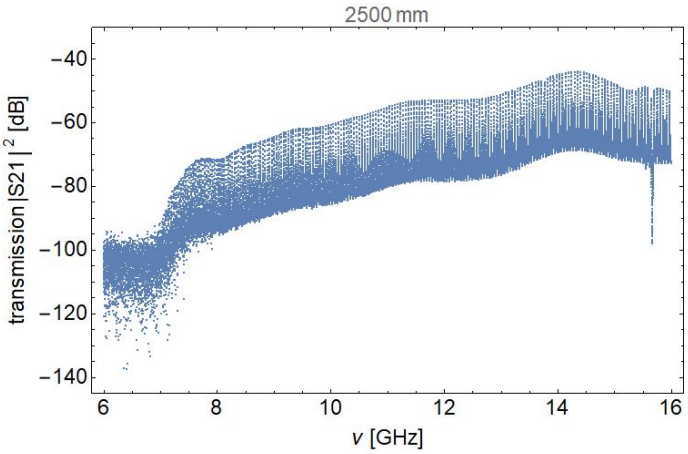

Figure 10: Modulus squared of the transmission coefficient S_{21} for a waveguide of length 2500 mm at RT as a function of frequency.

4.2 Measurements at cryogenic temperatures

At BT we choose 14 approximately equally distributed single modes within 7.6 GHz and 10.5 GHz and fit the transmission within a frequency range of around three times each the bandwidth at several input powers P_{in}.
We estimate quality factors of around $2.4 \cdot 10^6$ as plotted in Fig. 12 versus ν for an input power of -115 dBm. The attenuation constants α corresponding to the Q are plotted in Fig. 13. We extract attenuation constants of around $0.6\,\mathrm{dB\,km^{-1}}$, which corresponds to a 99.986 % signal transmission over 1 m or 99.655 % over 25 m.
In Fig. 14 α is plotted versus P_{in} for the mode at 8.365 GHz, where P_{in} is additionally related to the average number of photons $\bar{n}$ in the cavity. The attenuation constants as well as the quality factors are almost independent of P_{in} within the relevant power range of -155 dBm to -95 dBm to a good extent as can be seen in Fig.14.
The attenuation constant extracted in this experiment is smaller than the $0.005\,\mathrm{dB\,m^{-1}}$ mentioned in the introduction by one order of magnitude. An explanation for this might be that losses or imperfections at the input and output couplers become less important for a longer waveguide.
The model according Eq. (8) fits the data very well as exemplarily shown in Fig. 16. The estimated resonance frequencies coincide with the theoretical ones from Eq. (5) to a very good extent as can be seen in the mode number plot in Fig.15 in the appendix.

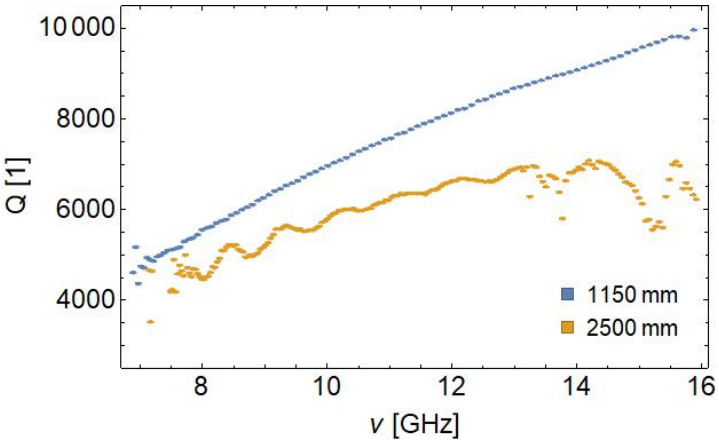

(a)

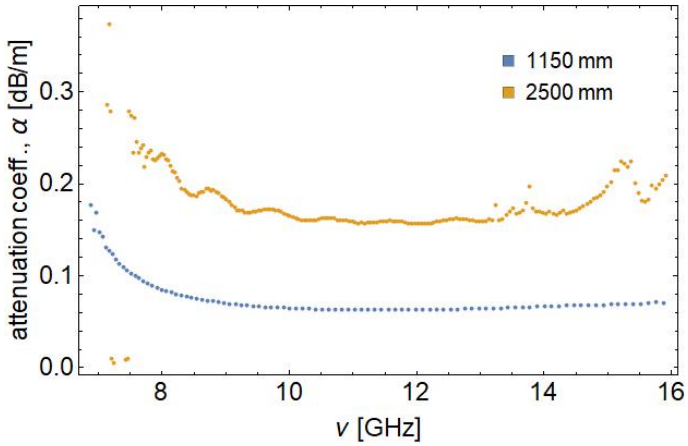

(b)

Figure 11: Quality factors Q in (a) and attenuation constants α in (b) for both waveguides at RT as a function of frequency.

A measurement of the background and the noise level around a resonance can be found in the appendix E. The transmissions we measure around modes are around 10 dB above the noise level, which indicates the reasonability of our data.

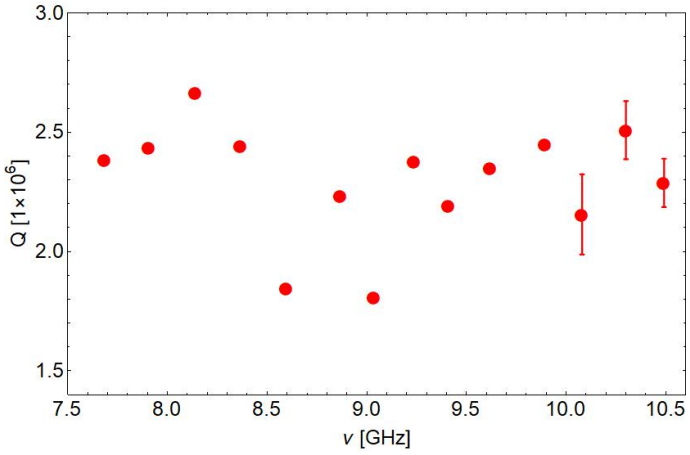

Figure 12: Quality factor Q of the waveguide in dependence of frequency ν for -115 dBm input power.

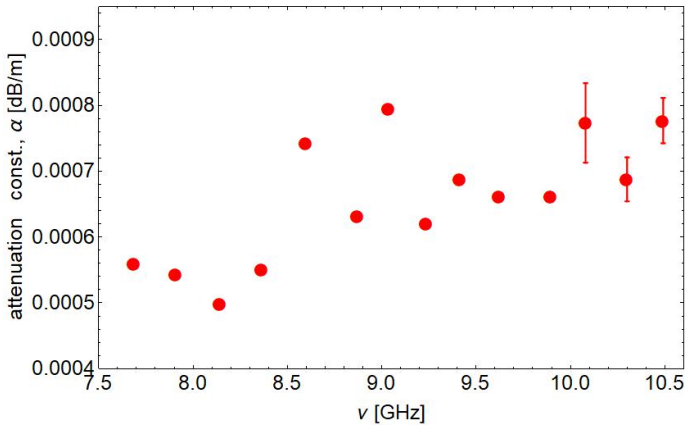

Figure 13: Attenuation constant α in dependence of frequency ν for -115 dBm input power.

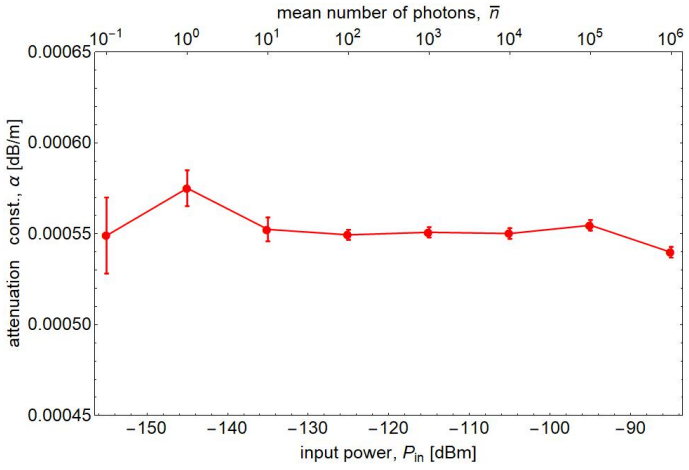

Figure 14: Input power P_{in} dependence of the attenuation constant α for the mode at 8.365 GHz. The input power can also be related to the average number of photons within the waveguide.

5 Conclusions

First the thermal anchoring of the waveguide is discussed using braids that are connected to the BT shield and clamped to the waveguide using thermal clamps. The thermal clamps aim to press braids and waveguide together to reduce the contact resistance. They consist of two stainless steel plates on each side and brass screws. By changing the thickness of the plates we are able to tune the stress between the plates and compensate for the effect of thermal expansion of all components compared to room temperature. We find a minimum thickness of 1.9 mm to keep the stress at cryogenic temperatures equal to the stress at RT. Moreover, the criterion that the screws must not break does not yield an upper limit for the thickness of the plates.
Furthermore, we analyze the thermal expansions of the waveguide and the BT shield components. Here, we find differences in length up to around 46 mm at the maximum due to thermal expansion, that are zero at RT, which must be taken into account to optimize the lengths of the braids.
Finally, we measure the performance of the thermalization in three different ways finding a temperature difference to the BT plate of around 80 mK for the best performing way of thermalization. As main reason for this imperfect thermalization we identify the small thermal conductivity of aluminium in its superconducting phase. Thus, we assume that even a tighter use of braids and clamps will not increase the thermalization significantly. A possible way to increase the thermalization might be to coat the waveguide for example with copper or a different material with higher thermal conductivity at millikelvin temperatures.
In the second part, we extract quality factors for the waveguide of length 3650 mm up to around $2.4 \cdot 10^6$ and attenuation constants down to $0.6\,\mathrm{dB\,km^{-1}}$ at millikelvin temperatures. Our results are one order of magnitude better than previous studies and are the first measurements of waveguides of length of several meters. The extracted attenuation constants indicate that around 99.66 % of a signal can be transmitted over a length of 25 m using the rectangular aluminium waveguide. A significant dependence of the attenuation constant on the input power is not found.
In recent measurements of compareable high quality 3D cavities quality factors up to $7 \cdot 10^7$ were found [11], so a better thermalization or a better surface treatment of the waveguide could improve the quality factors further.

A Linear thermal expansion parameters

For our calculations of thermal expansion we assume a final temperature of 1 K and use the linear expansion coefficients α given in Table 1, where the final temperature is already taken into account. One can then relate the original length l_0 at RT with the change of length Δl after cooling down according to

$$\Delta l = l_0 \alpha. \tag{3}$$

Material:	aluminium	copper	brass	stainless steel
α	$-4.15 \cdot 10^{-3}$	$-3.25 \cdot 10^{-3}$	$-3.85 \cdot 10^{-3}$	$-3.00 \cdot 10^{-3}$

Table 1: Linear expansion coefficients $\alpha = \Delta l/l$ of thermal expansion from RT to 1 K for several materials [12] [13].

B Displacements at several positions

In Table 2 the displacements between shield and waveguide are listed at several positions, where braids might be place. The position x is measured from the left as displayed in Fig.3.

Braid position x [m]	Δs [mm]
0.12	46.6
0.625	46.2
1.13	45.7
1.37	37.4
1.935	36.9
2.5	36.4
3.065	35.8
3.63	35.3
3.87	27.0
4.435	26.5
5	26.0
5.565	25.5
6.13	24.9
6.37	16.6
6.935	16.1
7.5	15.6
8.065	15.1
8.63	14.6
8.87	6.2
9.435	5.7
10	5.2
10.565	4.7
11.13	4.2

Table 2: Displacements Δs due to thermal expansion as discussed in section 2.2 at certain positions x, if $\Delta s = 0$ is assumed at RT.

C Mode numbers of resonance frequencies at RT and BT

The frequency range for the measurements at RT is between 6 GHz and 16 GHz, at cryogenic temperatures between 7.5 GHz and 10.5 GHz. The extracted resonance frequencies are plotted versus their mode numbers in Fig. 15a for RT and in Fig. 15b for BT. The solid lines correspond to the theoretical modes discussed in Eq. (5) for each length of the waveguide. As can be seen in Fig. 10, for frequencies around 7 GHz the resonances are below the noise level at RT. At both temperatures, the measured modes agree well with the theory, which justifies our further analysis discussed in section D.

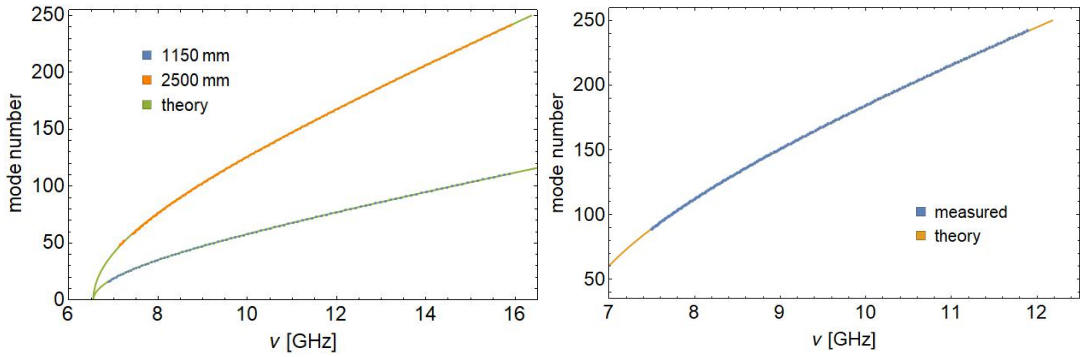

(a) (b)

Figure 15: Mode numbers of the measured resonance frequencies at RT in (a) and BT in (b).

D Analysis of the rectangular waveguide

In the this section we discuss how to extract the frequency dependent attenuation constant and the resonance frequencies from the measured transmission using the resonant-cavity technique.
The transverse electric modes (TE) of a rectangular waveguide are given by

$$\nu_{nmk} = \frac{c}{2\pi\sqrt{\varepsilon_\mathrm{r}\mu_\mathrm{r}}}\sqrt{\left(m\frac{\pi}{a}\right)^2 + \left(n\frac{\pi}{b}\right)^2 + \left(k\frac{\pi}{l}\right)^2}, \tag{4}$$

where ν_{mnl} is the frequency of the TE$_{mnk}$-mode, c the speed of light in vacuum, ε_r the relative permittivity, μ_r the relative susceptibility and a, b and l are the dimensions of the waveguide at the inside. Since the waveguide is filled with air in the RT measurements or in vacuum at cryogenic temperature, respectively, ε_r and μ_r are set to unity. Due to the geometry we only consider the TE$_{10k}$-modes, where a is the longer transverse direction and l is the length of the waveguide. Thus, the resonance frequencies can be simplified to

$$\nu_{10k} = \frac{c}{2}\sqrt{\left(\frac{1}{a}\right)^2 + \left(\frac{k}{l}\right)^2}. \tag{5}$$

In the experiment the complex transmission $S_{21}(\nu)$ as one component of the scattering matrix S is measured. Since waveguide and input and output couplers are aperture coupled, we can apply circuit theory to identify the microwave network with a weakly coupled parallel RLC circuit [12]. Thereby we find an expression for the complex transmission using the internal and external quality factors Q_i and Q_e as

$$S_{12}(\nu) = \left(\frac{1}{1 + Q_\mathrm{e}/Q_\mathrm{i} + 2iQ_\mathrm{e}(\nu/\nu_k - 1)} + X\right)e^{i\phi}. \tag{6}$$

Here, the complex constant X accounts for an impedance mismatch and ϕ regards a possible rotation of the data relative to the reference plane [14]. We extract the resonance frequencies ν_k and as the quality factors by simultaneously fitting the real and imaginary part of the data according Eq. (6).
As mentioned in the previous section, we ensure $Q_\mathrm{e} \gg Q_\mathrm{i}$ and therefore the largely undercoupled regime over the entire frequency range. We obtain Q_i from the loaded quality factor Q_1 in this regime

$$\frac{1}{Q_\mathrm{i}} = \frac{1}{Q_1} - \frac{1}{Q_\mathrm{e}} \approx \frac{1}{Q_1}. \tag{7}$$

Since we are able to at least ensure $Q_\mathrm{e} > 10Q_\mathrm{i}$ experimentally as discussed in section F of the appendix, this approximation is appropriate. As an advantage only Q_1 and the resonance frequencies ν_k need to be fitted, requiring only a fit of the absolute value

$$|S_{21}(\nu)| = \frac{{S_k}^{\max}}{\sqrt{1 + 4(\nu/\nu_k - 1)^2 {Q_1}^2}} + C_1 + C_2\nu. \tag{8}$$

The constant parameters C_1 and C_2 account for an offset and a small linear frequency dependence in the background [14]. Both parameters are most relevant for the small quality factors at RT. Sorting the data within a finite bandwidth around each resonance and fitting them each according to Eq. (8) is a precise method to estimate quality factors [14]. An example for this fit is presented in Fig. 16.

The frequency dependent internal quality factor of the $10k$-mode can be related to the surface resistance $R_\mathrm{S}(\nu_k)$ via [12]

$$Q_{\mathrm{TE}10k}(\nu_k) = \frac{2a^3 bl\pi\mu_0\nu_k^3}{R_\mathrm{S}(\nu_k)} \frac{1}{c^2 b(l-a) + 2a^3(2b+l)\nu^2}. \tag{9}$$

By fitting the internal quality factor and inverting Eq. (9) one can extract $R_\mathrm{S}(\nu_k)$. The attenuation constants $\alpha_{\mathrm{TE}_{10}}$ of the TE_{10} modes are related to the surface resistance according to [12]

$$\alpha_{\mathrm{TE}10}(\nu) = \frac{R_\mathrm{S}(\nu)}{a^2 b\mu_0 c} \frac{bc^2 + 2a^3\nu^2}{\nu\sqrt{4\nu^2a^2 - c^2}}. \tag{10}$$

E Background and noise level

In Fig. 17 the measured transmission background around a resonance at around 8 GHz is plotted, for the measurements the complex transmission for both an input signal for the

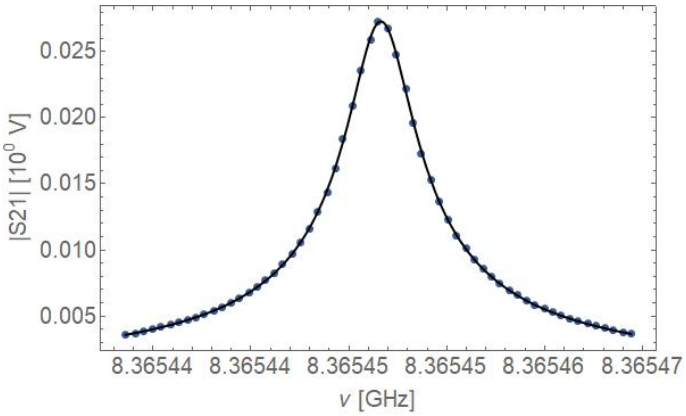

Figure 16: Example of a fitted mode at around 8.365 GHz using the fitting model discussed in the text, yielding a quality factor of $Q_1 = 2 \cdot 10^6$.

resonance background and without input signal for the noise background is measured. The measured noise level is approximately -10 dB below the transmission level of our actual measurements, which yields that the transmission measurements of the waveguide are significant and not only fluctuations. Moreover, the resonance is clearly in contrast to the background transmission by more than 40 dB.

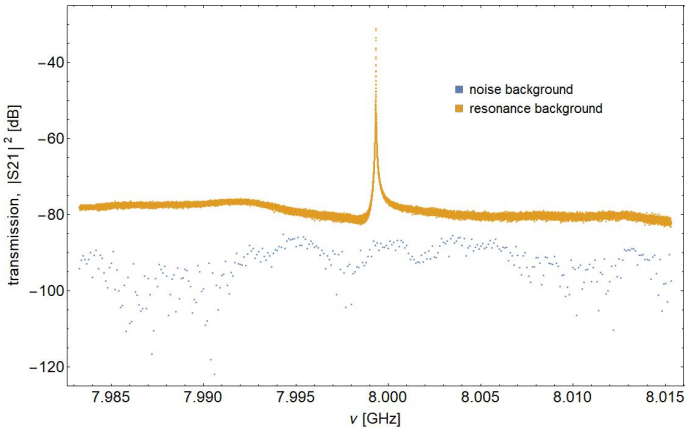

Figure 17: Background and noise level around a resonance at around 8 GHz.

F Measured external Quality factor

In Eq. 7 we assume a large external quality factor Q_e compared to the internal quality factor Q_i. If this relation is fulfilled, we can approximate the internal with the loaded quality factors, which is used for the fitting model. In section D we claim to ensure $Q_e > 10Q_i$ by tuning the coupling strength between the rectangular waveguide and the input or output couplers accordingly.
The measured Q_e versus ν are plotted in Fig. 18, indeed a factor of at least 30 or even higher between Q_e and Q is achieved as claimed. This justifies our earlier assumptions.

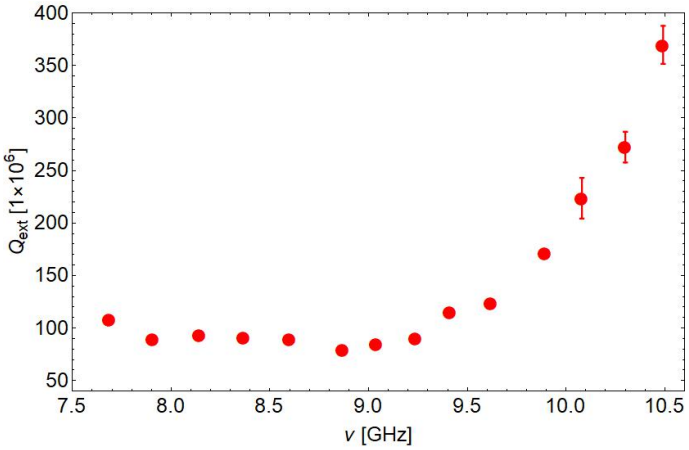

Figure 18: External quality factors Q_e measured for -115 dBm input power in dependence of frequency ν.

Acknowledgements

I would like to thank Professor Andreas Wallraff for giving me the opportunity to get an insight in the experimental work at the Quantum Device Lab and to perform my semester project here. My special thank you goes to my supervisor Philipp Kurpiers for all his helpful explanations on everything in great detail, be it on programming with Mathematica, getting used to Inventor, hands-on work in the lab or the theoretical backgrounds not only of my work. Moreover, I would like to thank Raphael Keller for his help with any of my technical problems and his tips for the CAD program. Finally, I would also like to thank Paul, both for his detailed explanations before as well as during my semester project and in the first place also for inviting me to the presentation of the possible projects in the group.

References

[1] David P. DiVincenzo. "The Physical Implementation of Quantum Computation". In: *Fortschritte der Physik* 48.9-11 (2000), pp. 771–783. DOI: 10.1002/1521-3978(200009)48:9/11<771::aid-prop771>3.0.co;2-e.

[2] P. Campagne-Ibarcq et al. "Deterministic remote entanglement of superconducting circuits through microwave two-photon transitions". In: *arXiv:1712.05854* (2017). URL: https://arxiv.org/abs/1712.05854.

[3] C. Axline et al. "On-demand quantum state transfer and entanglement between remote microwave cavity memories". In: *arXiv:1712.05832* (2017). URL: https://arxiv.org/abs/1712.05832.

[4] P. Kurpiers et al. "Deterministic Quantum State Transfer and Generation of Remote Entanglement using Microwave Photons". In: *ArXiv:1712.08593* (2017). arXiv: 1712.08593 [quant-ph]. URL: https://arxiv.org/abs/1712.08593.

[5] Philipp Kurpiers et al. "Characterizing the attenuation of coaxial and rectangular microwave-frequency waveguides at cryogenic temperatures". In: *EPJ Quantum Technology* 4.1 (2017). DOI: 10.1140/epjqt/s40507-017-0059-7.

[6] Penn Engineering Components. 2017. URL: http://www.pennengineering.com/.

[7] Louis J. Salerno and Peter Kittel. *Thermal Contact Conductance*. Tech. rep. Feb. 1997. URL: https://ntrs.nasa.gov/search.jsp?R=19970026086 (visited on 10/24/2016).

[8] Michael Prandl. *Vorspannkrfte und Anziehmomente fr Metrische Schrauben*. 2017. URL: http://www.schrauben-normen.de/anziehmomente.html.

[9] Robert E Collin. *Field theory of guided waves*. Oxford University Press, 1995.

[10] Christian Lang. "Quantum Microwave Radiation and its Interference Characterized by Correlation Function Measurements in Circuit Quantum Electrodynamics". PhD thesis. ETH Zurich, 2014.

[11] Matthew Reagor et al. "Reaching 10?ms single photon lifetimes for superconducting aluminum cavities". In: *Applied Physics Letters* 102.19 (2013), p. 192604. DOI: 10.1063/1.4807015. URL: https://arxiv.org/abs/1302.4408.

[12] David M Pozar. *Microwave engineering*. Wiley, 2012.

[13] *Cryogenic Material Properties*. 2017. URL: http://cryogenics.nist.gov/MPropsMAY/materialproperties.htm.

[14] Paul J. Petersan and Steven M. Anlage. "Measurement of resonant frequency and quality factor of microwave resonators: Comparison of methods". In: *Journal of Applied Physics* 84.6 (1998), pp. 3392–3402. DOI: 10.1063/1.368498.

ETH

Eidgenössische Technische Hochschule Zürich
Swiss Federal Institute of Technology Zurich

Declaration of originality

The signed declaration of originality is a component of every semester paper, Bachelor's thesis, Master's thesis and any other degree paper undertaken during the course of studies, including the respective electronic versions.

Lecturers may also require a declaration of originality for other written papers compiled for their courses.

I hereby confirm that I am the sole author of the written work here enclosed and that I have compiled it in my own words. Parts excepted are corrections of form and content by the supervisor.

Title of work (in block letters):

Characterizing the thermalization and attenuation of microwave waveguides at cryogenic temperatures

Authored by (in block letters):

For papers written by groups the names of all authors are required.

Name(s):	**First name(s):**
Meinhardt	Nicholas

With my signature I confirm that

- I have committed none of the forms of plagiarism described in the 'Citation etiquette' information sheet.
- I have documented all methods, data and processes truthfully.
- I have not manipulated any data.
- I have mentioned all persons who were significant facilitators of the work.

I am aware that the work may be screened electronically for plagiarism.

Place, date	**Signature(s)**
27.03.18, Zurich	N. Meinhardt

For papers written by groups the names of all authors are required. Their signatures collectively guarantee the entire content of the written paper.